IET Generation, Transmission & Distribution

Research Article

IET Journals
The Institution of Engineering and Technology

Frequency-dependent cable modelling for small-signal stability analysis of VSC-HVDC systems

ISSN 1751-8687
Received on 15th July 2015
Revised on 13th November 2015
Accepted on 5th February 2016
doi: 10.1049/iet-gtd.2015.0868
www.ietdl.org

Jef Beerten[1] ✉, *Salvatore D'Arco*[2], *Jon Are Suul*[2,3]

[1]*Department of Electrical Engineering (ESAT), Division ELECTA & Energyville, University of Leuven (KU Leuven), Heverlee, Belgium*
[2]*Department of Energy Systems SINTEF Energy Research, Trondheim, Norway*
[3]*Department of Electric Power Engineering, Norwegian University of Science and Technology (NTNU), Trondheim, Norway*
✉ *E-mail: jef.beerten@esat.kuleuven.be*

Abstract: State-of-the-art time-domain models of power cables account for the frequency dependency of physical parameters to enable accurate transient simulations of high-voltage transmission schemes. Owing to their formulation, these models cannot be directly converted into a state-space form as required for small-signal eigenvalue analysis. Thus, dc cables are commonly represented in high-voltage direct current (HVDC) power system stability studies by cascaded pi-section equivalents that neglect the frequency-dependent effects. This study demonstrates how the conventional cascaded pi-section model is unable to accurately represent the damping characteristic of the cable and how this can lead to incorrect stability assessments. Furthermore, an alternative model consisting of cascaded pi-sections with multiple parallel branches is explored, which allows for a state-space representation while accounting for the frequency dependency of the cable parameters. The performance of the proposed model is benchmarked against state-of-the-art cable models both in the frequency domain and in the time domain. Finally, the study provides a comparative example of the impact of the cable modelling on the small-signal dynamics of a point-to-point voltage-source converter (VSC) HVDC transmission scheme.

1 Introduction

The present trends for improving cross-border power market integration and the accelerating development of large-scale power production from renewable energy sources are generating a growing demand for high-voltage direct current (HVDC) transmission systems [1]. Moreover, voltage-source converter (VSC) HVDC technology is increasingly preferred due to the recent advances in efficiency and power rating [2, 3] combined with the inherent capability for reactive power or voltage control. Thus, even point-to-point HVDC transmission schemes for bulk power transfer are currently being developed and built using VSC technology [4, 5]. Furthermore, VSC HVDC can be especially relevant for the design of multi-terminal and even meshed grid configurations envisioned as a future offshore transmission grid in the North Sea region and as an overlay transmission grid in mainland Europe [6].

With the increasing penetration of HVDC transmission schemes in the existing ac grids, their accurate representation becomes critical when assessing power system dynamics and stability [7, 8]. For large-scale power systems, the small-signal stability is commonly studied using linearisation and corresponding eigenvalue analysis [9]. The underlying theory is well developed for stability phenomena related to the synchronous machines and their controllers, and tools are available in commercially graded power system software to study small-signal stability phenomena in ac power systems. Since the main dynamics of traditional large-scale power systems have been dominated by the inertial dynamics of the synchronous generators, these software tools are representing the ac grid by algebraic phasor models without accounting for any electromagnetic transients (EMTs). However, VSC HVDC systems are characterised by faster control loops and system dynamics. This has triggered research efforts in small-signal modelling and analysis of VSC HVDC systems during the last decade [10–15]. The focus has largely been on model development for interaction studies with the surrounding ac grid, whilst incorporating the dynamics of the ac and dc sides of the HVDC converter station. The behaviour of the dc cable in this respect, however, has been given less attention.

State-of-the-art frequency-dependent cable models for EMT simulations cannot be directly translated into a state-space representation needed for small-signal stability analysis. Therefore, it has been common practice to undertake small-signal stability studies with the dc cables represented as either a single pi-equivalent circuit [10–12, 15] or by multiple pi-equivalent circuits [13, 14]. In some cases, the internal dynamics of dc cables have been deliberately ignored by representing the dc transmission system as a resistive network [16]. In [17], the effect of this omission on the time-domain response was analysed, but again a single pi-equivalent cable model was used as a basis for comparison.

Recently, it was demonstrated in [18, 19] that conventional pi-equivalent representations for a dc cable can lead to a wrong stability assessment. The results presented in [19] also indicate that leaving out the cable current dynamics by omitting the inductance can at least avoid false conclusions regarding the stability of intermediate or high-frequency oscillations while retaining a reasonably accurate representation of the slower dynamics related to the overall power flow control. The need for representing the frequency-dependent characteristics of the dc cable for an accurate assessment of small-signal dynamics of HVDC transmission schemes was also confirmed by the findings in [19]. To account for the effect of frequency-dependent cable parameters on the oscillation modes and damping in small-signal studies, an HVDC cable model based on pi-equivalent sections with multiple parallel RL-branches was proposed in [19] as an alternative to the conventional cascaded pi-section state-space model [20]. The model is based on the approach presented in [21], which was applied for a state-space representation of transmission lines in [22]. The model parameter values were determined by vector fitting [23] and the order of the model could easily be adapted according to the accuracy requirements.

Starting from the approach presented in [19], this paper extends the analysis of the proposed model and demonstrates its

advantages and limitations by means of time-domain comparisons with a state-of-the-art EMT model. Such comparisons are presented for the model of a dc cable as well as for the analysis of a point-to-point HVDC link, verifying the ability of the proposed cable model to accurately represent the small-signal dynamics of the cable and its impact at a system level. Furthermore, it is shown that increasing the order of the conventional cascaded pi-section model by adding more sections does not improve the results, while a model with parallel RL-branches effectively can retain the damping characteristics of the actual cable, thereby preventing the prediction of non-existent instabilities.

2 Conventional cable modelling for state-space representation

In general, cable models can be classified into two main subgroups, based either on lumped parameters or on distributed parameters. In particular, the models with distributed and frequency-dependent parameters have proved to provide an accurate representation of the complex behaviour of power lines and cables [24]. Arguably the most established example of such a model is the universal line model (ULM) also known as wideband model [25]. The model benefits from efficient numerical implementations tailored to EMT analysis. Thus, the ULM is at present the preferred numerical implementation for time-domain simulation, as reflected by its availability in the standard libraries of commercial EMT software. Furthermore, it may be assumed as a reference to benchmark the performances of alternative models, as made clear by the time-domain comparison presented in [26]. Though suitable for time-domain simulations, the ULM and distributed parameter models in general, cannot be translated into a state-space representation for integration into larger models for performing small-signal eigenvalue analysis of power systems. For this class of applications, lumped parameters models are more common since they can be effectively and conveniently expressed in a state-space compatible format. However, a lumped parameter representation based on standard pi-equivalents fails to account for the frequency dependency of the parameters. This section summarises the conceptual steps that lead to the formulation of the conventional cascaded pi-section model for power cables. Moreover, the simplifying hypotheses that are embedded in the modelling approach are explicitly highlighted together with the resulting limitations that arise.

2.1 Steady-state cable model

For converter control interactions studies, the model of HVDC cables can be reduced by means of a Kron reduction. This assumes an ideal grounding for both the armour and sheath conductors: namely, that they are at ground potential along the entire length of the cable. In reality, the sheaths of subsea cables are usually grounded at both ends, while onshore cables can also be grounded at additional points along the length of the cable. Therefore, the reduction only applies when the voltages in armour and sheath remain small compared with the conductor voltage [27], which is a realistic assumption for control studies. As a consequence, the analytical representation of a subsea cable with three conducting layers (conductor, sheath and armour) reduces to that of an equivalent conductor. The cable can then be accurately described by the steady-state pi-model, as shown in Fig. 1.

The series and parallel elements of this circuit are given by

$$Z_\pi = z\ell \frac{\sinh\ \gamma\ell}{\gamma\ell} \tag{1}$$

$$Y_\pi = y\ell \frac{\tanh\left(\gamma\ell/2\right)}{\left(\gamma\ell/2\right)} \tag{2}$$

where ℓ is the length of the cable and z and y are the cable impedance

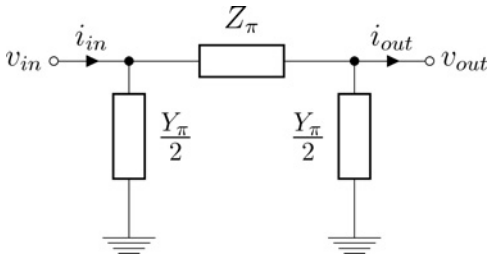

Fig. 1 *Steady-state pi-model of the cable*

and admittance per unit length, respectively

$$z(\omega) = r(\omega) + \mathrm{j}\omega l(\omega) \tag{3}$$

$$y(\omega) = g(\omega) + \mathrm{j}\omega c(\omega) \tag{4}$$

and γ is the propagation constant defined as

$$\gamma = \sqrt{zy} \tag{5}$$

The frequency dependency of the conductance g and the capacitance c is normally omitted for EMT models of power cables [27], simplifying (4) to

$$y = g + \mathrm{j}\omega c \tag{6}$$

On the contrary, omitting the frequency dependency of the resistance r and inductance l is much more severe, as discussed in the remainder of this paper. Figs. 2*a* and *b* show the frequency dependency of r and l for a 320 kV XLPE cable for VSC HVDC transmission with data from [28].

Figs. 2*c* and *d* show the impedance for a 300 km long cable with these parameters, using the analytical formulation from (1) to (6), with the cable short-circuited at one end.

2.2 Constant parameter approximation

An underlying assumption in the conventional cascaded pi-section model is that the frequency dependency of all parameters can be omitted, hence also simplifying (3) to

$$z = r + \mathrm{j}\omega l \tag{7}$$

It is important to stress that the resulting model still relies on the analytical formulation from (1) and (2), but with the approximation from (6) and (7).

Figs. 3*a* and *b* show the effect of removing this frequency dependency of r and l. In this example, the single values of these parameters are obtained by a weighted fitting over the frequency range of 1 µHz up to 1 MHz [23]. The process is described in more detail in Section 3.1. The overall result is an accurate representation of predominantly the low-frequency range.

2.3 Conventional cascaded pi-section model

As the model from the previous section still relies on the analytical formulation from (1) and (2), an approximation is needed to express it in a state-space format. A common approach is to use cascaded pi-sections. The approximation stems in the fact that for short lines, the hyperbolic correction factors in (1) and (2) approach 1, resulting in a series impedance $z\ell$. For longer lines, these correction factors can be approximated by cascading multiple pi-sections in series. This approach is taken in [20] to present a state-space model for transmission lines and is a commonly used approach to model HVDC cables for small-signal stability studies. Figs. 3*c* and *d* show the approximation of the cable with 1, 5 and 15 cascaded pi-equivalents, using the constant r and l values from Section 2.2.

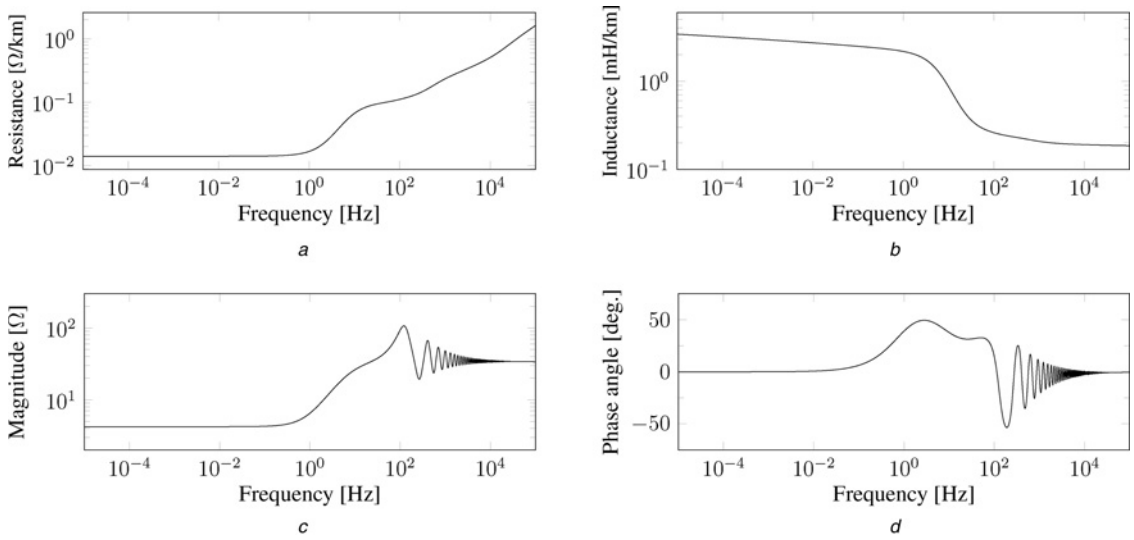

Fig. 2 *Frequency dependence of cable parameters and cable impedance*

a Cable parameters – resistance *r*
b Cable parameters – inductance *l*
c Steady-state cable model – impedance magnitude
d Steady-state cable model – impedance angle

These results clearly show that by cascading several branches the cable response better resembles the behaviour of the analytical equivalent pi-model with constant parameters (Figs. 3*a* and *b*), instead of the actual cable impedance (Figs. 2*c* and *d*).

3 Frequency-dependent cascaded pi-model

The previous discussion clearly highlights that increasing the number of pi-sections results in a better approximation of the hyperbolic correction factors from (1) and (2), but this does not result in a good approximation of the actual behaviour of the cable since it does not allow taking into account the frequency dependency of the distributed parameters. To overcome these drawbacks, the idea of modelling the cable by means of parallel series RL-branches from [21] has been used. In [22], this idea has been explored to include transmission lines in a state-space model. To some extent, the method presented in this paper also shows similarities to the approach taken in [18], which involved modelling the cable screen by including a coupled inductor. However, the proposed method is different since it assumes the screen to be at ground potential and is more general in the sense that the approach can be extended to an arbitrary number of branches, thereby improving the fitting in the frequency domain.

The modelling approach consists of two subsequent steps. First, the frequency dependencies of the series elements are fitted with parallel branches by using vector fitting [23]. Second, the hyperbolic correction factors from (1) and (2) are approximated with multiple pi-sections, resulting in the model from Fig. 4*a*.

The elements of the pi-equivalent scheme are given by

$$R_i = r_i \ell_\pi \tag{8}$$

$$L_i = l_i \ell_\pi \tag{9}$$

$$G = c\ell_\pi \tag{10}$$

$$C = g\ell_\pi \tag{11}$$

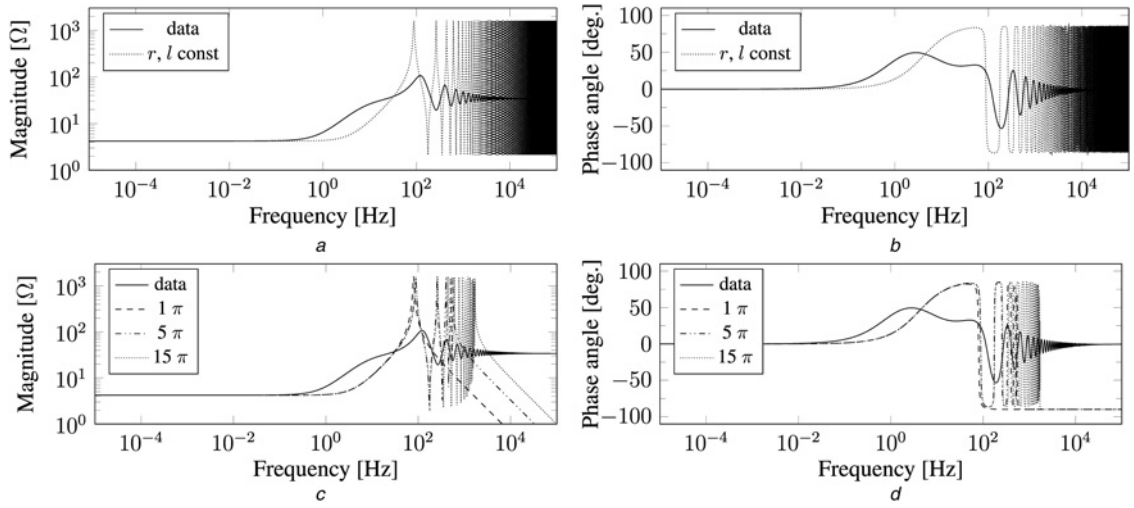

Fig. 3 *Cable impedance – constant parameter approximation and conventional pi-section model approximation*

a Constant parameter approximation – impedance magnitude
b Constant parameter approximation – impedance angle
c Conventional pi-section model – impedance magnitude
d Conventional pi-section model – impedance angle

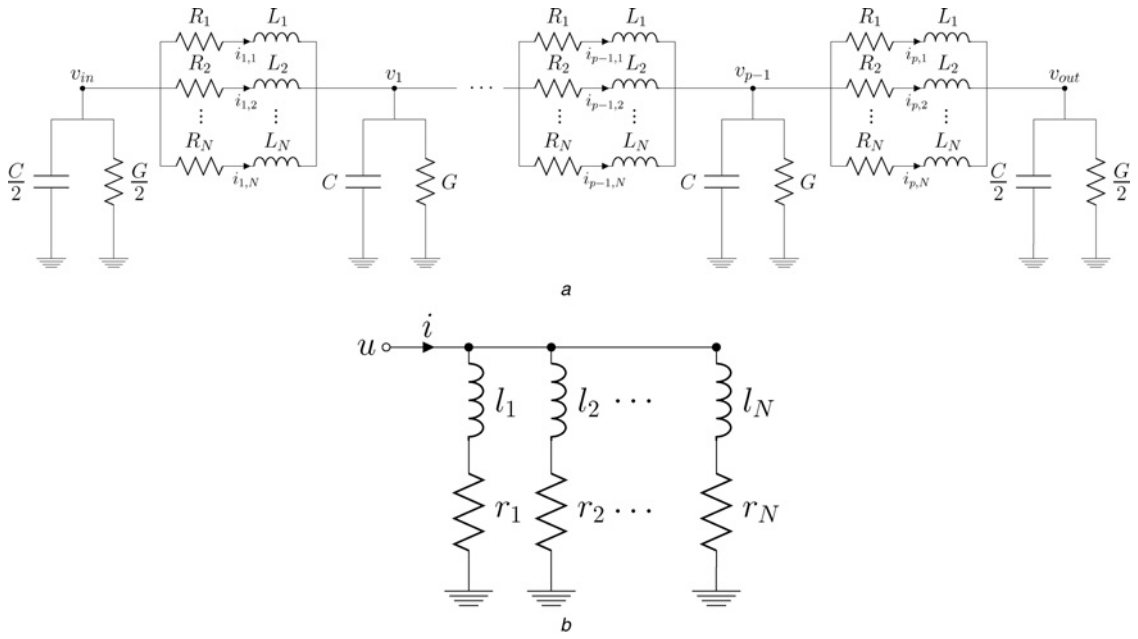

Fig. 4 *Cascaded pi-section model with parallel series branches*

a Full model
b Approximate representation of the frequency-dependent series parameters

where $\ell_\pi = \ell/p$ is the length of a pi-section and p represents the number of pi-sections.

3.1 Vector fitting of series impedance elements

The goal of the first step, the vector fitting, is to provide an adequate description of the series elements in the frequency domain by means of a rational approximation of order N. The problem takes the general form of a sum of partial fractions [23]

$$f(s) = \sum_{i=1}^{N} \frac{c_i}{s - a_i} + d + se \tag{12}$$

Considering N parallel branches with a resistance r_i and inductance l_i as in Fig. 4*b*, the series admittance of the cable, $y_s(s) = [r(s) + sl(s)]^{-1}$, is in fact approximated as

$$y_s(s) \simeq \sum_{i=1}^{N} \frac{1}{l_i s + r_i} \tag{13}$$

A comparison of (12) and (13) shows that this model naturally leads to a simplified version of the rational formulation from (12) with $d = 0$, $e = 0$ and

$$l_i = c_i^{-1} \tag{14}$$

$$r_i = -a_i c_i^{-1} \tag{15}$$

Hence, the dc resistance per unit length of the equivalent cable model is given by

$$r_{dc} = \frac{1}{\sum_{i=1}^{N} -a_i^{-1} c_i} \tag{16}$$

Figs. 5*a* and *b* show the approximation of the series impedance using five parallel branches.

The fitting of the series impedance data to parallel branches clearly provides a valid means to take into account the frequency dependence of the cable parameters.

3.2 Cascaded pi-section model with parallel branches

The hyperbolic correction factors in (1) and (2) are now taken into account by using cascaded pi-equivalents with parallel series branches. The number of pi-sections depends on the modelling needs and consequentially on the bandwidth of the cable model demanded in the state-space representation. This is illustrated in Figs. 5*c* and *d*, which show the results of using 1, 5 and 15 pi-sections for a cable model with five parallel branches.

The picture indicates that the method as such does not pose any theoretical restrictions on the level of detail that can be represented, but the model order increases with the number of pi-equivalents and the number of parallel branches.

3.3 State-space representation

The linear model from Fig. 4*a* can be directly written in a state-space form

$$\dot{\boldsymbol{x}}_c = \boldsymbol{A}_c \boldsymbol{x}_c + \boldsymbol{B}_c \boldsymbol{u}_c \tag{17}$$

with $\boldsymbol{x}_c \in \mathbb{R}^{n_c}$ as the cable state variable vector, $\boldsymbol{u}_c \in \mathbb{R}^2$ as the cable input vector and $\boldsymbol{A}_c \in \mathbb{R}^{n_c \times n_c}$, $\boldsymbol{B}_c \in \mathbb{R}^{n_c \times 2}$ as the cable coefficient matrices. Considering the cable separately, Fig. 4*a* can be represented by a state-space model by considering external current sources at both cable ends as inputs and the internal currents and voltages as states. In this paper, however, the cable is connected to a converter model with a capacitor at the dc side. Since in this case the dc voltages at both cable ends are already state variables of the converter, the shunt elements ($G/2$ and $C/2$ in Fig. 4*a*) of the pi-equivalents at the cable ends need to be treated as a part of the converter instead, by adding $C/2$ to the converter capacitance. Hence, for the general case of a cable with p pi-equivalents and N parallel branches the cable can be written as a state-space model with vectors $\boldsymbol{x}_c$ and $\boldsymbol{u}_c$ given by (18) and (21) and matrices $\boldsymbol{A}_c$ and $\boldsymbol{B}_c$ given by (19) and (20) respectively (see equations 18–20 at the bottom of next page).

$$\boldsymbol{u}_c = \begin{bmatrix} v_{in} \\ v_{out} \end{bmatrix} \tag{21}$$

The first and last sub-blocks of $\boldsymbol{A}_c$ in (19) differ as the voltages at the beginning and at the end of the cable are treated as inputs to the model [see $\boldsymbol{B}_c$ in (20)]. Similarly, in case only one pi-equivalent is used, matrices $\boldsymbol{A}_c$ and $\boldsymbol{B}_c$, respectively, simplify to an $N \times N$ and an $N \times 2$ matrix, with vector $\boldsymbol{x}_c$ only retaining the N currents as state variables.

3.4 Time-domain verification

In this section, different modelling approaches are compared by simulating a cable section in PSCAD/EMTDC. Cable geometries are taken from the open four-terminal test network presented in [28]. The cable has been implemented as ULM cable model, as well as using a model relying on a conventional cascaded pi-section approximation and the proposed cascaded pi-section model with parallel branches.

Figs. 6*a* and *b* show the open-circuit response of the different cable models. The ULM clearly shows the expected reflection patterns of the voltage at the cable ends. The conventional cascaded pi-section model with 15 pi-equivalents poorly represents the time response of the cable, resulting in a dominant oscillation with higher amplitude, much longer settling time and different oscillation frequency compared with the ULM's reflection pattern. The conventional pi-section model also results in high-frequency oscillations superimposed to the poorly damped low-frequency oscillation. The equivalent high-frequency dynamics are negligible in the ULM response, and are well damped for the models with parallel branches. It can be seen from these figures that all models with parallel branches provide a reasonably accurate representation of the open-end cable dynamics, with the most accurate results observed for the models with 15 pi-sections. The difference in response between the models with 5 and 9 parallel branches is negligible. It is also noted that among the models with parallel branches, the case with a single pi-section and five parallel branches has the lowest accuracy in representing the reflections at the cable ends: the model does not accurately represent the delayed increase in the voltage due to the travelling wave effect and has an initial peak value in the time response that is slightly lower than the other models. However, the oscillation frequency and settling time are much closer to the ULM model than those of the conventional cascaded pi-section model. Thus, a single section model with multiple parallel branches can more accurately represent the cable dynamics than a conventional model with multiple cascaded pi-sections.

Figs. 6*c* and *d* show the current through the cable for the different models after a step in the voltage of 1 V at one cable end with the other cable end short-circuited. No notable difference is observed

$$\boldsymbol{x_c} = \begin{bmatrix} i_{1,1} & \cdots & i_{1,N} & v_1 & i_{2,1} & \cdots & i_{2,N} & v_2 & \cdots & v_{p-1} & i_{p,1} & \cdots & i_{p,N} \end{bmatrix}^T \tag{18}$$

$$\mathsf{A_c} = \begin{bmatrix}
-\frac{R_1}{L_1} & & & -\frac{1}{L_1} & & & & & & & & & \\
& \ddots & & \vdots & & & & & & & & & \\
& & -\frac{R_N}{L_N} & -\frac{1}{L_N} & & & & & & & & & \\
\frac{1}{C} & \cdots & \frac{1}{C} & -\frac{G}{C} & -\frac{1}{C} & \cdots & -\frac{1}{C} & & & & & & \\
& & & \frac{1}{L_1} & -\frac{R_1}{L_1} & & & -\frac{1}{L_1} & & & & & \\
& & & \vdots & & \ddots & & \vdots & & & & & \\
& & & \frac{1}{L_N} & & & -\frac{R_N}{L_N} & -\frac{1}{L_N} & & & & & \\
& & & & \frac{1}{C} & \cdots & \frac{1}{C} & -\frac{G}{C} & -\frac{1}{C} & \cdots & -\frac{1}{C} & & \\
& & & & & & & & \ddots & \ddots & \ddots & & \\
& & & & & & & & \frac{1}{C} & \cdots & \frac{1}{C} & -\frac{G}{C} & -\frac{1}{C} & \cdots & -\frac{1}{C} \\
& & & & & & & & & & & \frac{1}{L_1} & -\frac{R_1}{L_1} & & \\
& & & & & & & & & & & \vdots & & \ddots & \\
& & & & & & & & & & & \frac{1}{L_N} & & & -\frac{R_N}{L_N}
\end{bmatrix} \tag{19}$$

$$\mathsf{B_c} = \begin{bmatrix} \frac{1}{L_1} & \cdots & \frac{1}{L_N} & & & \\ & & & -\frac{1}{L_1} & \cdots & -\frac{1}{L_N} \end{bmatrix}^T \tag{20}$$

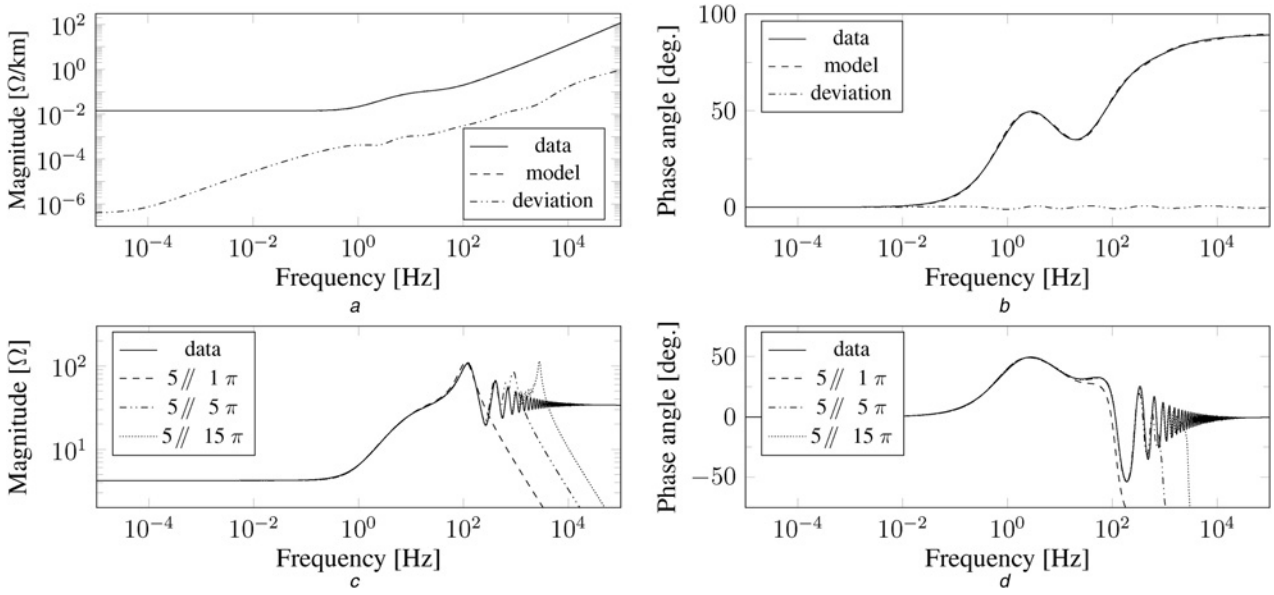

Fig. 5 *Cascaded pi-section model approximation – series impedance z and cable impedance using five parallel branches*

a Series impedance – impedance magnitude
b Series impedance – impedance angle
c Cable impedance – impedance magnitude
d Cable impedance – impedance angle

with respect to the number of pi-equivalents added. Indeed, the three curves representing the different models using five parallel branches, as well as the two models using nine parallel branches are largely overlapping. In general, all models correctly represent the steady-state behaviour (due to a good fitting at low frequencies), but the rise time is significantly different for the conventional cascaded pi-section model with 15 pi-equivalents. Furthermore, the resonances are also triggered to a much higher extent than in the other, more accurate models (Fig. 6*d*). The same oscillation frequencies as observed in Fig. 6*b* are excited for the conventional cascaded pi-section model, whereas the ULM and the pi-section models with multiple parallel branches show a smooth and well-damped response. Figs. 6*c* and *d* indicate that all models using parallel branches give a rather good approximation of the short-circuit response of the system. However, the number of parallel branches does alter the step response slightly and correspondence is best for the model with nine parallel branches (Fig. 6*c* – detail).

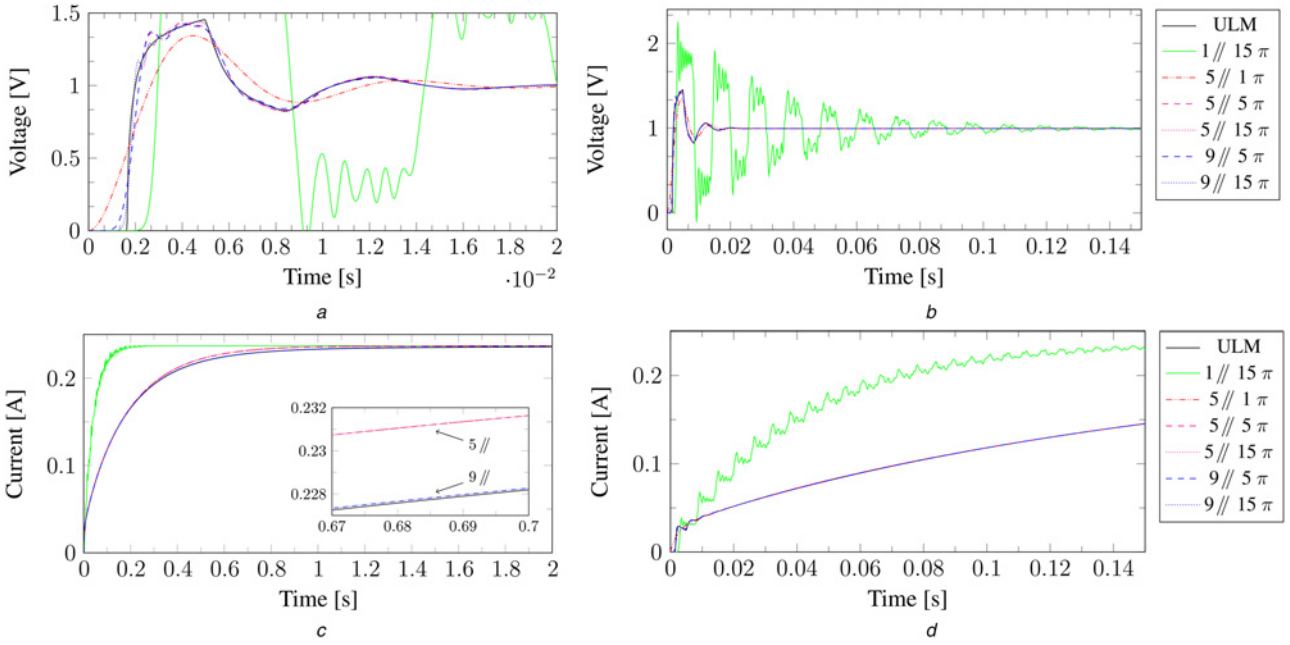

Fig. 6 *Time-domain cable model verification – open-circuit and short-circuit responses*

a Open circuit – step response (detail)
b Open circuit – step response
c Short circuit – step response (full response and detail)
d Short circuit – step response

4 Test system modelling

4.1 Reference configuration

To validate the proposed modelling approach, simulations are carried out for a ±320 kV, 900 MW two-terminal VSC HVDC link with a length of 300 km. Fig. 7*a* shows the system configuration, with converters *a* and *b*, respectively, set to constant voltage and constant power control.

The converter model used in this paper is based on the model described in [15], assuming an averaged model of a two-level converter including filter bus dynamics. The connection to the grid is taken into account using a complex impedance, which represents the combination of the transformer and the grid Thevenin impedance. Fig. 7*b* shows the averaged model that is used and indicates the different converter control loops.

A phase-locked loop is used to synchronise the *dq* reference frame to the voltage at the filter bus, whereas other control loops include decoupled inner current controllers and active power or dc voltage control. The structures of the outer control loops are depicted in Figs. 7*c* and *d*. The active power proportional–integral (PI) controller has been tuned to obtain an equivalent time constant of 25 ms (hence ten times slower than inner current controller), while the dc voltage controller has been tuned according to symmetric optimum tuning. Further features of the model include an active damping algorithm to prevent filter bus voltage oscillations from entering the control loops, as well as dynamics related to the low-pass filtering of dc voltage and active power measurements. The first-order measurement filters on the dc voltage and ac power signals have been tuned in order to obtain a 40 dB attenuation at the switching frequency, assumed to be 2.1 kHz. Outer control loops for the reactive power have been left out of the study. The current at the dc side is considered as an input to the converter model, as are the ac voltage source and the references for the controllers.

4.2 System state-space modelling

To write the non-linear converter model in a linear state-space form, the equations are linearised around a steady-state operation point $\boldsymbol{x}_0 \in \mathbb{R}^n$

$$\Delta\dot{\boldsymbol{x}} = \boldsymbol{A}\Delta\boldsymbol{x} + \boldsymbol{B}\Delta\boldsymbol{u}; \quad \boldsymbol{x}(0) = \boldsymbol{x}_0 \tag{22}$$

with $\Delta\boldsymbol{x} \in \mathbb{R}^n$ as the converter state vector, $\Delta\boldsymbol{u} \in \mathbb{R}^m$ as its input vector and $\boldsymbol{A} \in \mathbb{R}^{n\times n}$, $\boldsymbol{B} \in \mathbb{R}^{n\times m}$ as the coefficient matrices. The different components in the HVDC system are first modelled as independent linear time-invariant subsystems. With all different subsystems described in the form of (22), a state-space model of the entire system is assembled. To find the steady-state operation point for the entire system, which is needed to linearise the converter equations, a dc power flow solution is calculated, accounting for the dc system losses.

The overall system matrix $\boldsymbol{A}_\mathrm{t}$ can thereafter be assembled by accounting for the state variables of the different models that are input variables to the model of other components. More specifically, these are the dc currents at the cable ends and the converter dc voltages.

The total state-space model is given by

$$\Delta\dot{\boldsymbol{x}}_\mathrm{t} = \boldsymbol{A}_\mathrm{t}\Delta\boldsymbol{x}_\mathrm{t} + \boldsymbol{B}_\mathrm{t}\Delta\boldsymbol{u}_\mathrm{t} \tag{23}$$

with

$$\Delta\boldsymbol{x}_\mathrm{t} = \left[\Delta\boldsymbol{x}_a{}^\mathrm{T} \quad \Delta\boldsymbol{x}_b{}^\mathrm{T} \quad \Delta\boldsymbol{x}_c{}^\mathrm{T}\right]^\mathrm{T} \tag{24}$$

$$\Delta\boldsymbol{u}_\mathrm{t} = \left[\Delta\boldsymbol{u}_a^{r\,\mathrm{T}} \quad \Delta\boldsymbol{u}_b^{r\,\mathrm{T}}\right]^\mathrm{T} \tag{25}$$

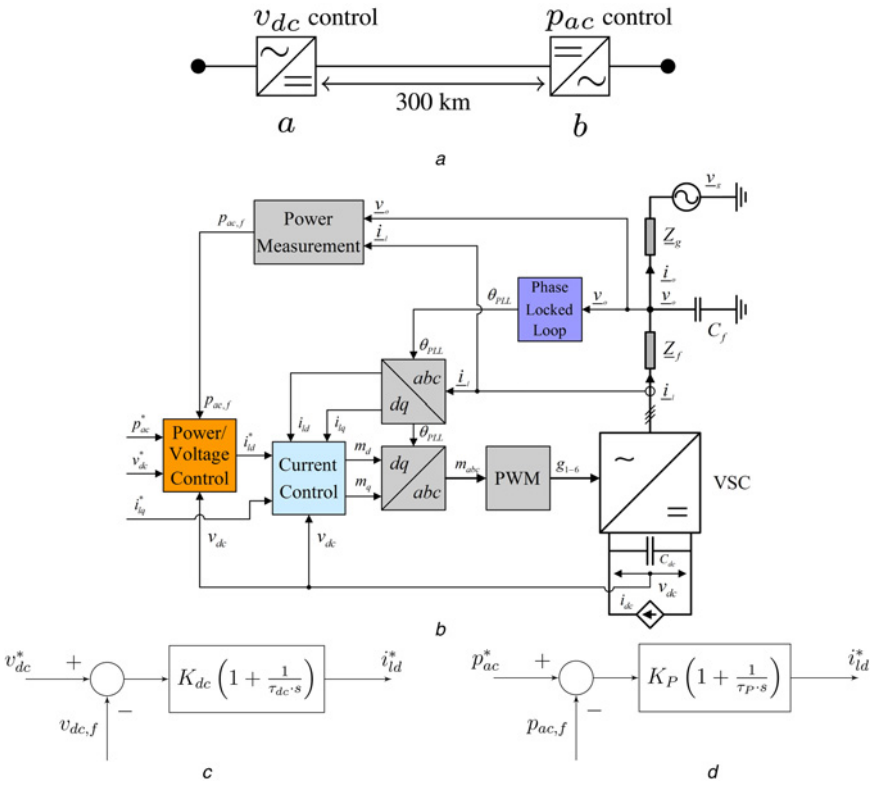

Fig. 7 *System modelling and control implementation*

a Two-terminal test system configuration
b Converter model
c Constant dc voltage control loop
d Constant power control loop

For this two-terminal HVDC system, subscripts a, b and c, respectively, refer to the first and second converters and the cable connecting the two converters.

Without overlapping states in the modelling of the components, $\Delta \boldsymbol{x}_t \in \mathbb{R}^{n_t}$ with $n_t = n_a + n_b + n_c$. The total input vector $\Delta \boldsymbol{u}_t \in \mathbb{R}^{m_t}$ only consists of reduced versions $\Delta \boldsymbol{u}_a^r \in \mathbb{R}^{m_a}$, $\Delta \boldsymbol{u}_b^r \in \mathbb{R}^{m_b}$ of the converter input vectors $\Delta \boldsymbol{u}_a \in \mathbb{R}^{m_a}$ and $\Delta \boldsymbol{u}_b \in \mathbb{R}^{m_b}$, since the dc currents and voltages are no longer inputs to subsystem models, but state variables of the cables and converters, respectively.

5 Impact of cable model on system interactions

5.1 Identification of interaction modes

Following the procedure presented in [19], this paper uses the concept of interaction modes to identify the system interactions in the test system and to address the effect of the cable modelling on these modes. These interaction modes are defined as those system modes in which the two converters participate. Using participation factors as defined in [9], let p_{ki} denote the participation factor of state variable x_k in mode i, $\boldsymbol{p}_i \in \mathbb{R}^{n_t}$ the vector with the participation factors for all system states associated with mode i and $\boldsymbol{p}_{\alpha,i} \in \mathbb{R}^{n_\alpha}$ the vector with the participation factors for all states of subsystem α. A parameter $\eta_{\alpha i}$ is now defined as a measure for the overall participation for each subsystem α in mode i such that

$$\eta_{\alpha i} = \frac{\|\boldsymbol{p}_{\alpha,i}\|}{\|\boldsymbol{p}_i\|} \tag{26}$$

with $\|\cdot\|$ denoting the L_1-norm. η_{ai}, η_{bi} and η_{ci} are a measure for the degree to which the two converters and the cable participate in each mode. Using a threshold χ, we define an interaction mode i as a mode for which both $\eta_{ai} > \chi$ and $\eta_{bi} > \chi$, resulting in a subset of interaction modes $\mathcal{S}$.

5.2 Interaction analysis with cascaded pi-section model with parallel branches

Fig. 8*a* shows the eigenvalues of $\boldsymbol{A}_a$ (converter a), the dc voltage controlling converter. The bandwidth of both converter models f_B is equal to 581 Hz. The states that are mainly associated with these modes are resulting from the LC circuit at the ac side, and hence little impact on their position can be expected when connecting the cable. The conservative assumption that the model for the cable needs to be accurate until this frequency, results in a cable model with 9 parallel branches and 15 pi-sections. Thus, the impedance angle deviation is limited to less than 0.5° in the low-frequency region and is limited to 2° at f_B. Similarly, the impedance magnitude deviation is limited to 7% at f_B. Fig. 8*b* shows the resulting eigenvalues for the combined system. The eigenvalues with real parts lower than -10^3 and

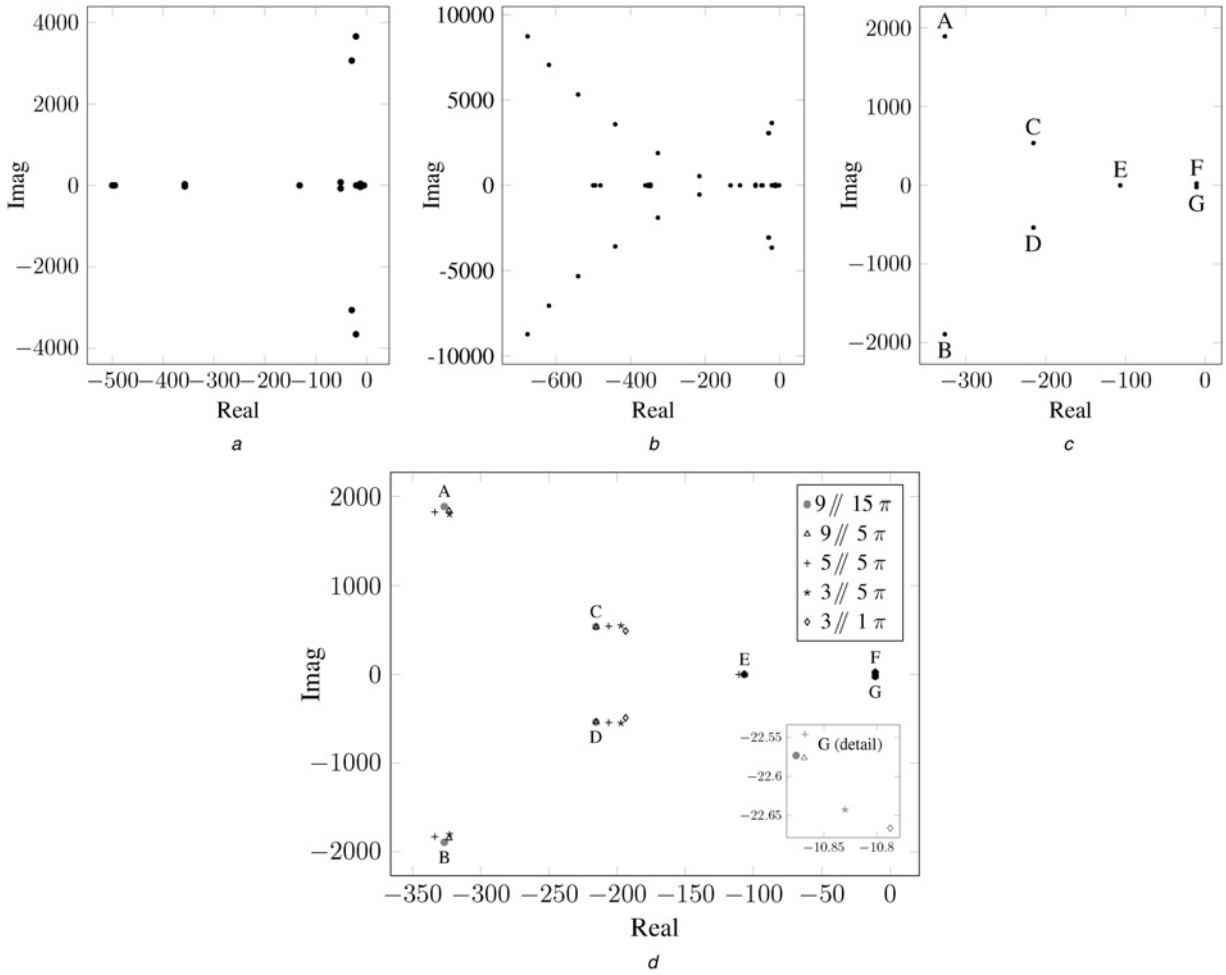

Fig. 8 *System, converter and interaction modes and cable model reduction*

a Eigenvalues $\boldsymbol{A}_a$ (converter a)
b Eigenvalues $\boldsymbol{A}_t$ (system)
c Interaction modes – eigenvalues $\boldsymbol{A}_t$ with $\eta_a > 5\%$ and $\eta_b > 5\%$
d Cable model reduction preserving interaction modes

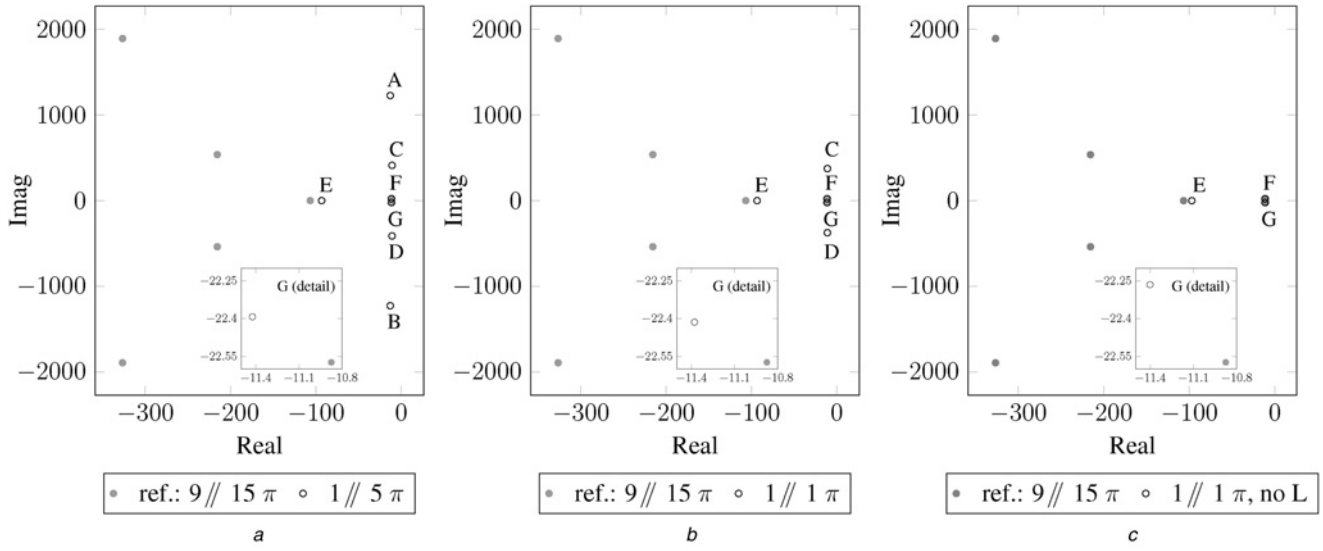

Fig. 9 *Conventional cable state-space representations and their effect on the interaction modes (reference case: 9 parallel branches, 15 cascaded pi-sections)*

a Cascaded pi-section approximation
b Single pi-section approximation
c Single pi-section approximation without inductance

imaginary parts over 10^4 have not been depicted in this figure as these modes are well-damped and mainly related to internal cable states. Fig. 8*c* shows eigenvalues that are the result of the interaction study after defining $\eta_{\alpha i}$ for the different components α for mode i with a threshold $\chi = 5\%$. In total, seven interaction modes are identified between the two converters.

The required cable bandwidth is now reduced to 297 Hz, corresponding to the frequency of the highest interaction mode of interest. Fig. 8*d* shows the effect of lowering the number of parallel branches and pi-sections. The figure shows that a model with five parallel branches and five pi-equivalents provides a good compromise to still accurately represent the eigenvalues of interest. The picture indicates that keeping the number of parallel branches equal to nine whilst lowering the number of pi-sections, leaves the poles C–G largely unaltered and only impacts A and B, the poles with the highest imaginary parts. Lowering the number of parallel branches to five, impacts the poles C and D as well. The number of parallel branches can be lowered to three, which forms a lower limit to still represent the complex conjugate poles A and B. It is clear from this picture that including a number of parallel branches whilst only using one pi-equivalent still allows a reasonably accurate representation of the poles C and D. It is also clear from Fig. 8*d* (see detail) that all models accurately represent the interaction modes F and G, with the lowest accuracy for the simplest models with only three parallel branches. These models are slightly conservative with respect to the damping of modes C, D, F and G and can in this case still be used for stability assessment.

5.3 Conventional state-space cable modelling effects on interaction modes

The result of the simplifications that are commonly encountered in state-space representation and their effect on the placements of the poles involved in the interaction modes are shown in Fig. 9.

It is clear from this figure that the simplifications based on using one parallel branch (and either one or multiple pi-sections) give misleading impressions about the relative stability of the cable modes (denoted A, B, C and D in Fig. 8*c*): the corresponding eigenvalues not only appear at different frequencies, but are also poorly damped. The representation of the lower-order cable modes is also less accurate than the representations from Fig. 8*d*, and even than the model using one pi-section and three parallel branches. Similarly, the representation of the real pole (*E* in Fig. 8*c*) is less accurate. It can be noted that the simplest representation, only using the resistive cable value and leaving out the current as a state variable (Fig. 9*c*), results in similar values for modes E, F and G,

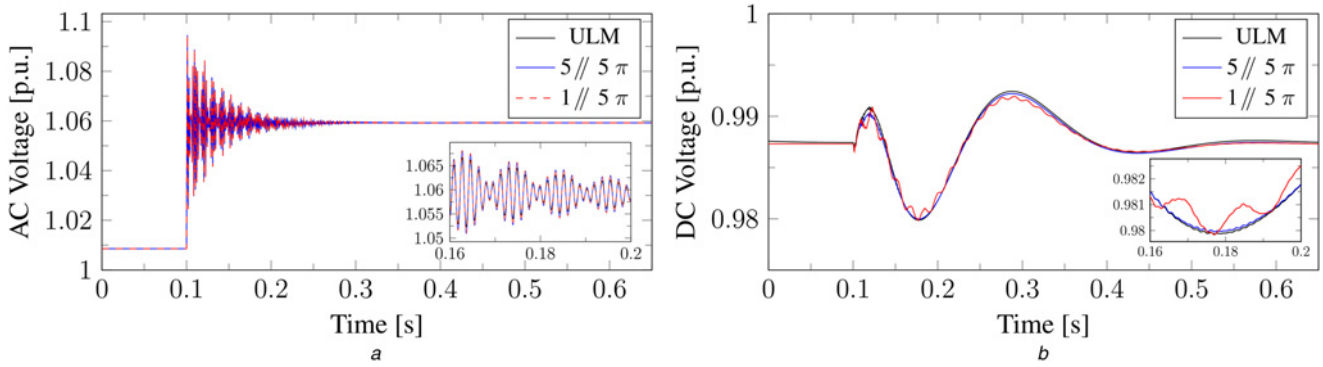

Fig. 10 *Time-domain comparison of linearised model with non-linear two-terminal model with ULM cable model – ac voltage step change (0.1 pu) at power controlling converter*

a Filter capacitor voltage (*d*-component)
b dc voltage

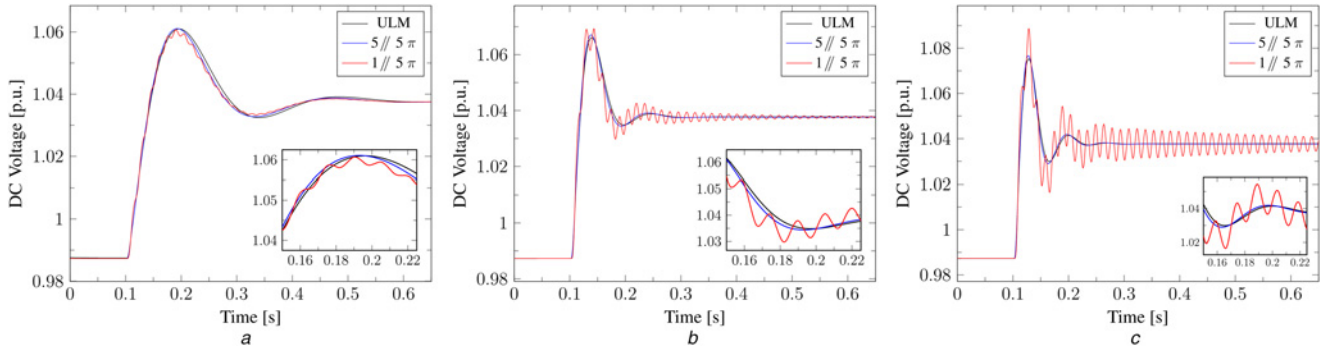

Fig. 11 *Time-domain comparison of linearised model with non-linear two-terminal model with ULM cable model – dc voltage reference step change (0.05 pu), voltage at the power controlling converter*

a Symmetric optimum controller tuning
b Increased dc voltage controller gains (K_{dc} scaling factor 3)
c Increased dc voltage controller gains (K_{dc} scaling factor 4.85)

but does not include the wrongly predicted oscillatory modes from the conventional (cascaded) pi-section models.

6 Cable modelling effects on dynamic response and system stability

The state-space models are verified against a time-domain model using MATLAB/Simulink. The overall aim is to illustrate how the typical time response of the two-terminal system changes when the frequency dependency of the cable parameters is accounted for in the state-space model or when, alternatively, a conventional cascaded pi-model is used. The 'benchmark' study case is a non-linear three-phase averaged model in MATLAB/Simulink SimPowerSystems, with the cable implemented using the WideBand Line model from the OPAL-RT ARTEMiS-SSN library.

The results of the benchmark model have been compared against the response of a linear state-space model using a cable model with five parallel branches and five pi-sections, as well as the conventional cascaded pi-model with five pi-sections. Fig. 10 shows the response of the system when subjected to a 10% step change of the equivalent ac grid voltage at the power controlling converter station. From Fig. 10*b*, it is clear that the step change in ac voltage causes an oscillation of the dc voltage in the system.

Comparing the results of the conventional cascaded pi-section model with the others, it is clear that the perturbation at the ac side triggers a poorly damped oscillation at the dc side which is not present in the ULM model and in the model with parallel branches. The small differences between the ULM model and the cascaded pi-section model with parallel branches are mainly a result of the linearised state-space modelling when operating away from the linearisation point. On the ac side, the two linearised models show a good match with the non-linear averaged model.

In a next step, the effect of the cable modelling on the stability analysis of the system is investigated by scaling the controller gain K_{dc} of the dc voltage PI controller (Fig. 7*c*). Fig. 11 shows the dc voltage response at the power controlling converter after a 5% step change in the dc voltage reference with different controller tuning. Under symmetric optimum controller tuning (Fig. 11*a*), the erroneous dc voltage oscillations are mainly present during the initial phase of the step response and do not significantly influence the time response. When increasing both PI gains by factors of, respectively, 3 (Fig. 11*b*) and 4.85 (Fig. 11*c*), the oscillations become more and more persistent and will eventually lead to instability in the conventional cascaded pi-section model when increasing the controller gains even further.

Fig. 12 shows clearly that adding more pi-sections, which results in an increased bandwidth of the cable model, does not result in a more realistic time-domain response, hence confirming the results from Fig. 9. There is almost no notable difference between the models with 5, 15 and 25 pi-sections (Fig. 12*a*) and also the model with a single pi-section indicates a similar oscillatory pattern (Figs. 12*b* and *c*). The time-domain response of the single pi-section model with the inductance omitted does not suffer from the wrongly predicted oscillation, but faces a slightly lower overshoot and a somewhat faster response than the ULM model (Fig. 12*b*). None of the conventional pi-section models succeed in representing the system response as accurately as the cascaded pi-model with parallel branches (Fig. 11).

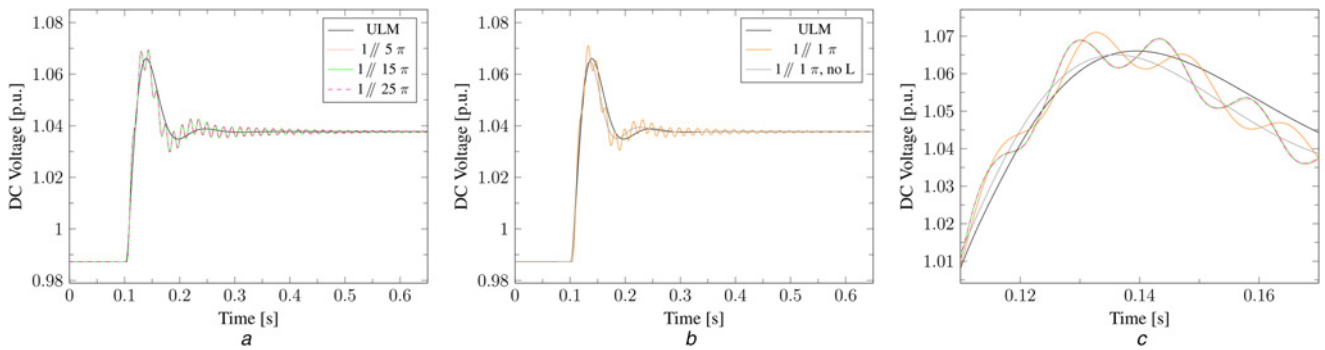

Fig. 12 *Time-domain comparison of different conventional cascaded pi-section models with ULM cable model for K_{dc} scaling factor equal to 3 – dc voltage reference step change (0.05 pu), voltage at the power controlling converter*

a Cascaded pi-section model
b Single pi-section model, with and without inductances
c Detail including all models from (a) and (b)

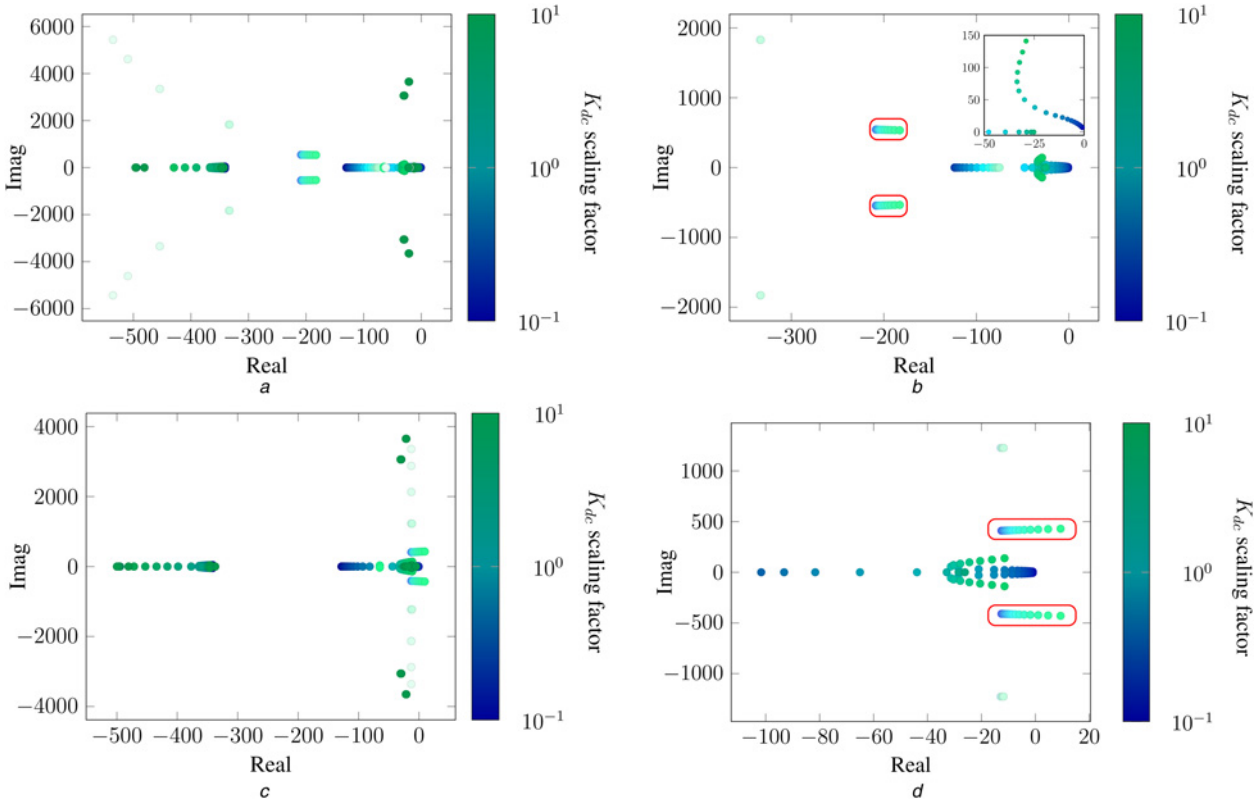

Fig. 13 *Change of system modes and interaction eigenvalues when changing the voltage controller gain K_{dc}*

a All modes – five parallel branches, five pi-sections
b Interaction modes – five parallel branches, five pi-sections
c All modes – conventional cascaded pi-section model, five pi-sections
d Interaction modes – conventional cascaded pi-section model, five pi-sections

Finally, Fig. 13 shows the effect of this parameter variation on the location of the overall system modes (Figs. 13*a* and *c*) and on the interaction modes (Figs. 13*b* and *d*) in particular when changing gain K_{dc} of the dc voltage controller (Fig. 7*c*) at converter *a* from 0.1 to 10 times the original settings. The intensity indicates the participation of the converters in these modes: the lighter, the more the mode is related to the cable, the darker, the more it is related to the converters. Changing the gains slightly alters the interaction pattern (Figs. 13*b* and *d*) in terms of new poles appearing compared with the results from the previous sections. These real poles are related to the integrator of the dc voltage controller at converter *a* and the dc filtered voltage at this converter, as well as with the dc voltages at both cable ends. Comparing the interaction pattern from Figs. 13*b* and *d* confirms the time-domain analysis. Namely, an increase of the controller gains causes the poles which are strongly linked to the first cable resonance (modes *C* and *D* from Fig. 9*a*, encircled in Fig. 13*d*) to move into the right-hand plane, hence making the system unstable for the case of the conventional cascaded pi-section model. On the other hand, in the model with parallel branches (Fig. 13*b*), the poles linked to the first cable resonance (modes *C* and *D* from Fig. 8*d*) do not trigger any instability and are still well damped, even for the higher controller gain settings. From the overall system poles in Figs. 13*a* and *c*, it is clear that no other system instabilities are triggered when changing the gains, other than the wrongly represented dc resonance in case of using conventional cascaded pi-section models. Investigation of the participation factors of these unstable modes shows that they are about equally linked with the dc voltages at both converters, and with internal cable state variables. This confirms that the pole becomes unstable because of a wrongly represented interaction between the converter controls and a cable resonance that is well damped in reality, but poorly damped in a conventional cascaded pi-section model.

7 Conclusion

In this paper, the effect of the frequency dependency of HVDC cables on the small-signal stability has been assessed. The traditional state-space models generally encountered in the literature using the conventional cascaded pi-section modelling result in a poor representation of the cable modes in the frequency domain. This can lead to false conclusions on the dynamic response and stability margin of HVDC systems. As an alternative, a model with parallel branches based on a vector fitting of the series elements of the cable has been proposed to account for the frequency dependency of the cable parameters. The model allows for an accurate representation of the cable in the frequency domain and provides a time-domain response similar to that of wideband cable models. Furthermore, the approach can also be applied for other line or cable configurations. It is shown that the model accurately represents the system interaction modes with a lumped parameter model designed to cover the frequency range at which such interactions can occur. The study leads to the general conclusion that the cable should preferably be modelled by a combination of parallel branches and pi-sections. In case a very simple model is sought for, it is better to model the cable using only parallel branches instead of merely cascading pi-sections.

8 Acknowledgments

The authors thank B. Gustavsen (SINTEF Energy Research) for his assistance with the vector fitting tool and W. Leterme (KU Leuven) for providing the cable data. Jef Beerten is funded by a postdoctoral research grant from the Research Foundation – Flanders (FWO). The work of SINTEF Energy Research in this paper was supported by

the project 'Protection and Fault Handling in Offshore HVDC Grids – ProOfGrids', financed by the Norwegian Research Council together with industry partners EDF, National Grid, Siemens, Statkraft, Statnett, Statoil and NVE.

9 References

1 European Network of Transmission System Operators for Electricity (ENTSO-E): 'Ten-year network development plan 2014'. Final Report, 2014

2 Judge, P., Merlin, M., Mitcheson, P., *et al.*: 'Power loss and thermal characterization of IGBT modules in the alternate arm converter'. Proc. IEEE ECCE 2013, Denver, USA, 15–19 September 2013, pp. 1725–1731

3 Barnes, M., Beddard, A.: 'Voltage source converter HVDC links – the state of the art and issues going forward', *Energy Procedia*, 2012, **24**, pp. 108–122, selected papers from Deep Sea Offshore Wind R&D Conference, Trondheim, Norway, 19–20 January 2012

4 Francos, P., Verdugo, S., Alvarez, H., *et al.*: 'INELFE – Europe's first integrated onshore HVDC interconnection'. Proc. IEEE PES GM 2012, San Diego, USA, 22–26 July 2012, p. 8

5 Callavik, M., Lundberg, P., Hansson, O.: 'NORDLINK – pioneering VSC-HVDC interconnection between Norway and Germany'. White Paper, March 2015

6 Van Hertem, D., Ghandhari, M.: 'Multi-terminal VSC HVDC for the European supergrid: obstacles', *Renew. Sustain. Energy Rev.*, 2010, **14**, (9), pp. 3156–3163

7 Gnanarathna, U.N., Gole, A.M., Jayasinghe, R.P.: 'Efficient modeling of modular multilevel HVDC converters (MMC) on electromagnetic transient simulation programs', *IEEE Trans. Power Deliv.*, 2011, **26**, (1), pp. 316–324

8 Saad, H., Peralta, J., Dennetiere, S., *et al.*: 'Dynamic averaged and simplified models for MMC-based HVDC transmission systems', *IEEE Trans. Power Deliv.*, 2013, **28**, (3), pp. 1723–1730

9 Kundur, P.: 'Power system stability and control' (McGraw-Hill Inc., New York, 1993)

10 Prieto-Araujo, E., Bianchi, F.D., Junyent-Ferre, A., *et al.*: 'Methodology for droop control dynamic analysis of multiterminal VSC-HVDC grids for offshore wind farms', *IEEE Trans. Power Deliv.*, 2011, **26**, (4), pp. 2476–2485

11 Pinto, R., Rodrigues, S., Bauer, P., *et al.*: 'Operation and control of a multi-terminal DC network'. Proc. IEEE ECCE Asia 2013, Melbourne, Australia, 3–6 June 2013, pp. 474–480

12 Pinares, G., Tjernberg, L., Tuan, L.A., *et al.*: 'On the analysis of the dc dynamics of multi-terminal VSC-HVDC systems using small signal modeling'. Proc. IEEE PowerTech 2013, Grenoble, France, 16–20 June 2013, p. 6

13 Wang, W., Barnes, M., Marjanovic, O.: 'Droop control modelling and analysis of multi-terminal VSC-HVDC for offshore wind farms'. Proc. IET ACDC 2012, Birmingham, UK, 4–6 December 2012, p. 6

14 Chaudhuri, N., Majumder, R., Chaudhuri, B., *et al.*: 'Stability analysis of VSC MTDC grids connected to multimachine AC systems', *IEEE Trans. Power Deliv.*, 2011, **26**, (4), pp. 2774–2784

15 D'Arco, S., Suul, J.A., Molinas, M.: 'Implementation and analysis of a control scheme for damping of oscillations in VSC-based HVDC grids'. Proc. PEMC 2014, Antalya, Turkey, 21–24 September 2014, p. 8

16 Kalcon, G.O., Adam, G.P., Anaya-Lara, O., *et al.*: 'Small-signal stability analysis of multi-terminal VSC-based DC transmission systems', *IEEE Trans. Power Syst.*, 2012, **27**, (4), pp. 1818–1830

17 Beerten, J., Cole, S., Belmans, R.: 'Modeling of multi-terminal VSC HVDC systems with distributed DC voltage control', *IEEE Trans. Power Syst.*, 2014, **29**, (1), pp. 34–42

18 Rault, P.: 'Dynamic modeling and control of multi-terminal HVDC grids'. PhD dissertation, Ecole Centrale de Lille, March 2014

19 Beerten, J., D'Arco, S., Suul, J.A.: 'Cable model order reduction for HVDC systems interoperability analysis'. Proc. IET ACDC 2015, Birmingham, UK, 10–12 February 2015, p. 10

20 Rosendo Macías, J., Gómez Expósito, A., Bachiller Soler, A.: 'A comparison of techniques for state-space transient analysis of transmission lines', *IEEE Trans. Power Deliv.*, 2005, **20**, (2), pp. 894–903

21 Semlyen, A., Deri, A.: 'Time domain modelling of frequency dependent three-phase transmission line impedance', *IEEE Trans. Power Appl. Syst.*, 1985, **PAS-104**, (6), pp. 1549–1555

22 Garcia, N., Acha, E.: 'Transmission line model with frequency dependency and propagation effects: a model order reduction and state-space approach'. Proc. IEEE PES GM 2008, Pittsburgh, USA, 20–24 July 2008, p. 7

23 Gustavsen, B., Semlyen, A.: 'Rational approximation of frequency domain responses by vector fitting', *IEEE Trans. Power Deliv.*, 1999, **14**, (3), pp. 1052–1061

24 Marti, J., Marti, L., Dommel, H.: 'Transmission line models for steady-state and transients analysis'. Proc. Athens Power Tech (APT) 1993, September 1993, vol. 2, pp. 744–750

25 Morched, A., Gustavsen, B., Tartibi, M.: 'A universal model for accurate calculation of electromagnetic transients on overhead lines and underground cables', *IEEE Trans. Power Deliv.*, 1999, **14**, (3), pp. 1032–1038

26 Beddard, A., Barnes, M.: 'HVDC cable modelling for VSC-HVDC applications'. Proc. IEEE PES GM 2014, Washington DC, USA, 27–31 July 2014, p. 5

27 Gustavsen, B., Noda, T., Naredo, J., *et al.*: 'Power system transients: parameter determination' (Taylor and Francis Group, 2010), pp. 137–175, Ch. 3

28 Leterme, W., Ahmed, N., Beerten, J., *et al.*: 'A new HVDC grid test system for HVDC grid dynamics and protection studies in EMT-type software'. Proc. IET ACDC 2015, Birmingham, UK, 10–12 February 2015, p. 7